A R C H I V E O F M E C H A N I C A L E N G I N E E R I N G

Volume 67 2020 Number 2

DOI: 10.24425/ame.2020.131687

Key words: laminated aluminum structure, axial drop, buckling, three-point bending, flexural response, delamination

Jifeng Wang[1], Tyler P. Morris[1], Reza Bihamta[1], Ye-Chen Pan[1]

Numerical and experimental verification of impact response of laminated aluminum composite structure

Laminated Aluminum Composite Structure (LACS) has shown great potential for replacing traditional bulk aluminum parts, due to its ability to maintain low manufacturing costs and create complex geometries. In this study, a LACS, that consists of 20 aluminum layers joined by a structural tape adhesive, was fabricated and tested to understand its impact performance. Three impact tests were conducted: axial drop, normal and transverse three-point bending drop tests. Numerical simulations were performed to predict the peak loads and failure modes during impacts. Material models with failure properties were used to simulate the cohesive failure, interfacial failure, and aluminum fracture. Various failure modes were observed experimentally (large plastic deformation, axial buckling, local wrinkling, aluminum fracture and delamination) and captured by simulations. Cross-section size of the axial drop model was varied to understand the LACS buckling direction and force response. For three-point bending drop simulations, the mechanism causing the maximum plastic strain at various locations in the aluminum and adhesive layers was discussed. This study presents an insight to understand the axial and flexural responses under dynamic loading, and the failure modes in LACS. The developed simulation methodology can be used to predict the performance of LACS with more complex geometries.

1. Introduction

With the automotive industry moving towards electrification, reduction of vehicle mass proves critical in increasing the range of electric vehicles. Laminated materials are capable of reducing vehicle part mass, while still maintaining a high specific strength. This gives laminated materials an integral role in the vehicle design process moving forward. In addition to their ability to reduce mass, laminated

✉ Jifeng Wang, e-mail: Jifeng.wang@gm.com

[1]General Motors Global Technical Center, 29360 William Durant Boulevard, Warren, Michigan 48092-2025, USA.

materials are also capable of creating complex geometries, helping to make the low volume production vehicles profitable.

Aluminum is a frequently used material in automotive design, but there has yet to be data generated indicating the performance of laminated aluminum structures. In order to implement laminated aluminum structures into the vehicle design process, the structural responses need to be fully understood and a simulation methodology needs to be developed. Previous studies looking at metallic laminate structures have been able to model their responses numerically using experimental test data, further supporting the idea of an aluminum laminate structure [1–7]. A study by Yu et al. [2] experimentally and analytically evaluated the static and low velocity impact behavior of sandwich beams with metallic foam between the top and bottom plates. Their modified Gibson's model was able to predict the average loads quite accurately. Research done by Dhaliwal and Newaz [4] resulted in a low velocity impact model of Carbon Fiber Reinforce Aluminum Laminates. LS-Dyna software enabled the model to possess intralaminar failure, delamination for composites, and application of strain-based failure mode for the base aluminum. The intralaminar is caused by matrix cracking along fibers within layers. Dhaliwal and Newaz also used the cohesive elements for modeling the delamination in the laminated parts. Sun et al. [3] presented a multi-scale computational analysis method of unidirectional carbon fiber reinforced polymers under various loading conditions. In their study, they used the cohesive elements for a numerical simulation of interfacial debonding and characterized interfacial debonding by reverse engineering based on their tests.

Modeling the material's performance is critical in today's vehicle development process, since engineering design relies heavily on simulations. The cost it takes to conduct full vehicle, or even component level tests, is immensely greater than the cost to run and iterate on a simulation. Because of the cost benefit, it is important to be able to accurately model new materials and structures. If a model is not able to predict failure and material responses during dynamic loading, it is unlikely that that material will be implemented into a vehicle due to potential liability and risk.

A previous study explored the experimental and numerical analysis of laminated aluminum composite structures (LACS) for quasi-static conditions [8]. However, since the crashworthiness load cases are always critical in a vehicle design, the present study explored the dynamic loading response of laminated aluminum parts using drop tower tests. Like previous studies on laminate structures, drop tests for axial and three-point bending in the normal direction were conducted [9–15]. Yang et al. [10] experimentally tested the material properties and failure mechanics of woven fiber-reinforced aluminum alloy composites with two different compositions. They used three-point bending and micro-structural evaluation to analyze their samples. Kinawy et al. [11] evaluated the buckling of composites after delamination for aeronautical applications. Kaboglu et al. [12] evaluated high-velocity impact deformation and perforation of fiber metal laminates by four-point quasi-static and high-velocity impactors. Wang et al. [13] evaluated the interlaminar

shear behavior of basalt fiber reinforced polymer (FRP) and Hybrid FRP laminates. The interlaminar failure takes place between two layers within a laminate. In their experiments, they used three-point bending to evaluate the different fracture modes for composites and the crack initiation and delamination modes. Yapici and Metin [15] evaluated the effect of low velocity post-impact buckling, as well as damage of various composites at different energy levels. Their results showed that impact-induced delamination can significantly reduce the compressive strength of the structures.

These types of tests provide the results needed to match the loading response and dynamic failure modes. One difference in the tests conducted in this study compared to the field, was three-point bending in the transverse direction, shown in Fig. 1. Since parts in crash scenarios experience different loading directions and combinations, it was felt that conducting tests in the axial, normal, and transverse direction would best capture the loading responses and dynamic failure modes seen in a crash event. These tests provide the necessary information to develop a robust model that can be used to analyze full vehicle crash events. With this understanding and well-engineered designs, testing and developmental costs can be reduced.

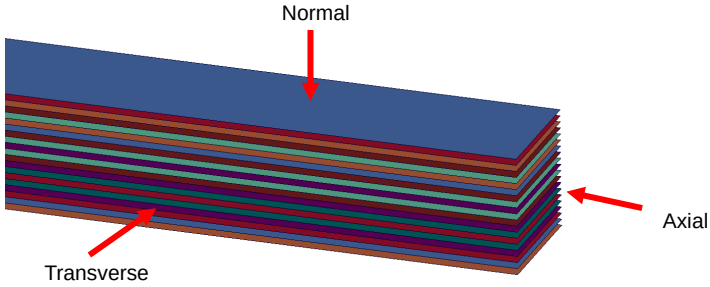

Fig. 1. A model schematic indicating the three loading directions performed during drop tower tests (Axial, Normal, and Transverse)

2. Experiments

2.1. Testing sample preparation

Large AA6111-T4 aluminum sheets with a thickness of 2 mm were cut into samples using a shear machine. To measure the aluminum properties and check the level of anisotropy, tensile tests at 0, 45, and 90 degrees with respect to the rolling direction were performed. It was confirmed that anisotropy could be neglected, and the aluminum could be considered isotropic. To make sure the mechanical property measurements were accurate, the tensile test samples were heat treated in the same curing condition as the adhesive (explained below). The resultant stress-strain curves were very similar to the typical properties reported for AA61111-T4 [16]. In addition, a single-layer epoxy-based tape adhesive (SAT1010) was cut

to the same size as the aluminum test samples by the tape supplier [17]. This tape adhesive was developed by 3M and was mainly designed for body in white (BIW) applications in the automotive industry. The recommendation for this tape adhesive was that it is not essential to do any additional surface preparation on the aluminum surface for automotive applications.

Two aluminum sheets were then stacked and attached using the tape adhesive. The tape adhesive was applied in accordance with the supplier's directions, to make sure there was no air trapped in between the aluminum and tape adhesive [17]. This process was repeated until the desired sample thickness was achieved. In addition, samples were machined very slowly to remove the overflow of the tape adhesive from the exterior surfaces of the samples to ensure a uniform sample geometry.

The recommended minimum curing time for the tape adhesive (SAT1010) is fifteen minutes at 165°C [17]. However, due to the multi-layer structure of the components and the lower thermal conductivity of the adhesive, it was expected that the central layers of the adhesive might not satisfy the minimum curing time at the specified temperature. To overcome this potential issue, a thermo-couple was inserted in the middle of one sample and a timer was used to determine how long it would take for the middle layer to reach 165°C. After this time limit was captured, fifteen minutes were added to this time to establish the total curing time for the test samples. This duration ensures that the minimum curing time will be reached for all layers in every test sample. The adhesive supplier (3M) assured that experiencing longer curing time for the exterior layers would not cause issues. Completed axial and three-point bending samples are shown in Fig. 2. The respective length, width, thickness, and number of aluminum layers are listed in Table 1.

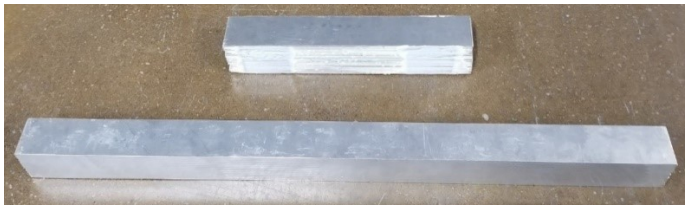

Fig. 2. Top: Axial drop test sample. Bottom: Three-point bending sample used for normal and transverse loading

Table 1.

Testing sample dimensions

Test type	Length (mm)	Width (mm)	Thickness (mm)	No. of Al layers
Axial drop	290	52	44	20
Normal drop	700	52	44	20
Transverse drop	700	44	52	20

2.2. Testing procedure

Three types of dynamic testing were conducted on the LACS using a drop weight impact tower, shown in Fig. 3. The types of drop tests run were an axial test, a three-point bending test (normal), and a three-point bending test with the sample rotated 90 degrees (called transverse three-point bending in this study). The axial drop fixture is depicted in Fig. 4 and has a square opening with bolts threaded into it from all four sides to allow samples of different thicknesses to be tested. The bottom 50 mm of the 290 mm sample was placed into the fixture and two of the four bolts (top and right) were tightened to the point where there was no movement or gap between the sample and the fixture. The other two screws (left and bottom) were left flush with the fixture to allow the sample to rest against the left and bottom sides. This helped increase repeatability with varying sample sizes. The fixture was securely bolted down for testing.

(a)

(b)

Fig. 3. (a) Axial drop tower setup; (b) Three-point bending drop tower setup

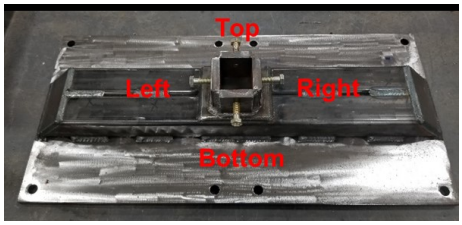

Fig. 4. Axial drop tower fixture. The screws were used to adjust for various samples sizes. The fixture gripped the bottom 50 mm of the sample

The three-point bending fixture, illustrated in Fig. 5, was designed in two symmetrical pieces to allow the span length to be adjusted. The fixture was securely bolted down at a set distance, so that when the 700 mm sample was placed in the fixture, 100 mm of the sample rest in each side of the fixture's channels, resulting in a 500 mm span length between the fixtures. The sample was not affixed within the channel, which allowed the sample to slide and freely rotate about the cylindrical tubes at the end of the channel during loading. These cylindrical tubes were used so that the sample deformed in a traditional three-point bending scenario and the channels were implemented to prevent the sample from translating or rotating in directions other than that of the impactor's motion. Spacers were placed within the fixtures channels to ensure that the sample was straight.

Fig. 5. Three-point bending fixture. This fixture was designed in two separate pieces to allow for various spans. The fixture allowed the samples to slide and rotate about the end rollers during loading

The axial drop samples, 290 mm long and 52 mm wide, were impacted at 9.8 m/s with an impactor weight of 269 kg. Loading occurred after the impactor struck the sample and ended when the velocity of the impactor reached zero. The three-point bending tests were conducted at a drop velocity of 10.0 m/s and 11.1 m/s with an impactor weight of 271 kg. The impactor struck the sample directly in the center and deformation occurred until the impactor's velocity decreased to zero. The test conditions are summarized in Table 2. The impactors were instrumented with an 7231c Endevco accelerometer (Farmington Hills, MI) and a triaxial load cell (Robert A Denton, Plymouth MI) to capture the event. The data was recorded using a TDAS PRO Sim system (Diversified Technical Systems, Seal Beach CA)

and filtered at a CFC of 180. The velocity and displacement data were derived from the accelerometer. A high-speed video camera made by Redlake (San Diego, CA) with a frame rate of 1000 fps was used to observe the deformation pattern and delamination during the crash events.

Table 2.

Drop tower test conditions

Test type	Drop velocity (m/s)	Drop weight (kg)	Span length (mm)
Axial	9.8	269	–
Three-point Normal	10.0	271	500
Three-point Transverse	11.1	271	500

3. Simulations

Laminated composite structures can fail structurally, interfacially and cohesively. Fig. 6 depicts each one of these failure modes. The aluminum was modeled in LS-Dyna using *MAT_24, which is an elasto-piecewise linear plasticity model. A generalized incremental stress state dependent material damage model (GISSMO) is needed when modeling this aluminum in vehicle crash simulations because it allocates accurate material failure properties and shows the gradual damage accumulation extracted from material testing [18, 19]. The damage accumulation used is determined by Equation (1) [4, 20],

$$\Delta D = \frac{DMGEXP}{\varepsilon_f} D^{\left(1-\frac{1}{DMGEXP}\right)} \Delta\varepsilon_p \,, \tag{1}$$

where, D represents the damage value from 0 to 1, ε_f is failure plastic strain, ε_p symbolizes the equivalent plastic strain increment, and $DMGEXP$ is the exponent

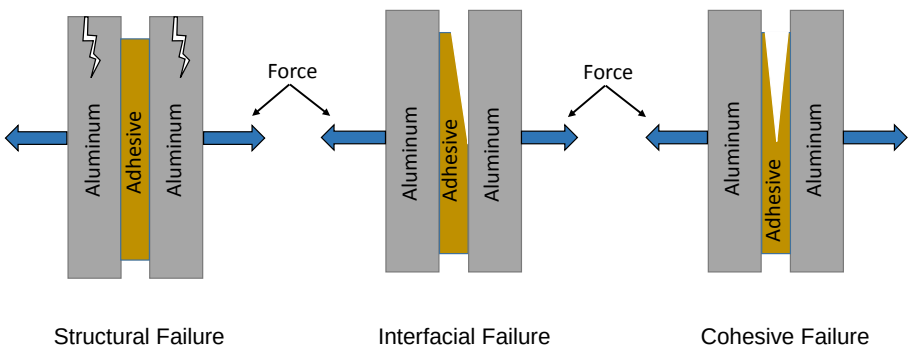

Fig. 6. Three failure modes of the laminated aluminum structures (structural, interfacial, and cohesive)

for nonlinear damage accumulation. The strain rate effect is not considered in the material model.

Interfacial and cohesive failure both cause delamination. Delamination is the failure of bonds within the adhesive, or a failure of the bonds to the substrate [4, 21]. LS-DYNA *MAT_169 was used to model the adhesive in the simulations, since it was developed for adhesive bonding to aluminum. Unlike the traditional elasto-plastic material model, the plasticity model in MAT_169 is not volume-conserving, which can avoid the spuriously high tensile stresses applied in adhesive. The *MAT_169 material card defines maximum shear and tensile stresses. These properties couple with a power law, Equations (2) and (3), to predict the yield and failure surfaces [20]. This failure is used to capture the cohesive failure mode in the model.

$$\left(\frac{\sigma}{\sigma_{\max}}\right)^{PWRT} + \left(\frac{\tau}{\tau_{\max} - SHT\_SL * \sigma}\right)^{PWRS} = 1.0, \tag{2}$$

where, σ and $\sigma_{\max}$ symbolize the direct stress and max direct stress respectively, τ and $\tau_{\max}$ represents the shear stress and max shear stress respectively, *SHT_SL* is the slope of yield surface at zero tension, *PWRT* is the power law for tension, and *PWRS* indicates the power law term for shear.

$$d_{ft} = 2\left(\frac{GCTEN}{TENMAX}\right), \tag{3}$$

where, d_{ft} indicates the displacement needed for failure in tension, *GCTEN* symbolizes the energy per unit area to fail the bond in tension, and *TENMAX* is the maximum through-thickness tensile stress.

Fig. 7 illustrates the yielding surfaces. Yielding occurs when the shear stress and direct stress exceed the *SHT_SL* = 0 curve. Shear and tension failure criterion are depicted in Fig. 8. The adhesive fails cohesively when the failure displacement is met [20, 22].

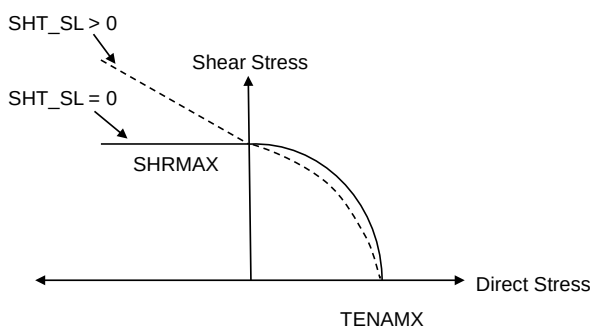

Fig. 7. Power-law relationship to determine yielding in the material using tensile and shear stresses

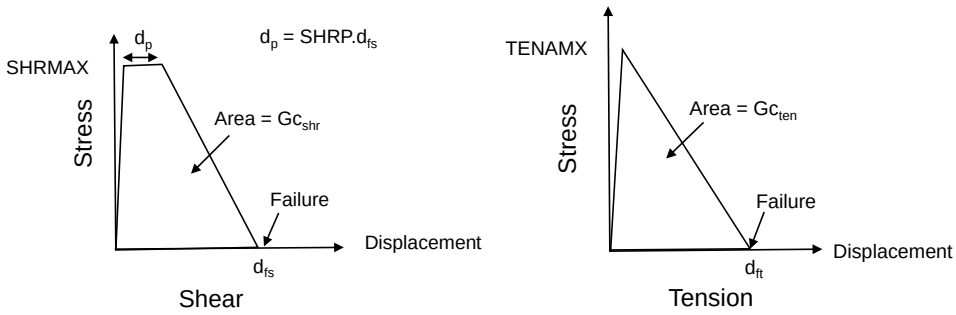

Fig. 8. Failure displacements for shear and tensile stresses

The interfacial failure mode was captured by defining a tiebreak contact with normal and shear failure stresses between the adhesive and the aluminum substrate. During loading, the damage of the adhesive in this contact operates as a linear function of the distance between the two originally contacted points [23]. When the tiebreak contact fails, it switches to a surface to surface contact to avoid penetrations. The failure criterion for a tiebreak contact is shown in Equation (4) [20]:

$$\left(\frac{|\sigma_n|}{NFLS}\right)^2 + \left(\frac{|\sigma_s|}{SFLS}\right)^2 \geqslant 1 \tag{4}$$

where, σ_n represents the normal stress, *NFLS* stands for the tensile failure strength, σ_s symbolizes the shear stress, and *SFLS* is the shear failure strength.

The laminated aluminum sample was modeled with 20 aluminum layers and 19 adhesive layers. Each aluminum layer was modeled using shell elements and the adhesive in between each aluminum layer was modeled using solid elements as shown in Fig. 9.

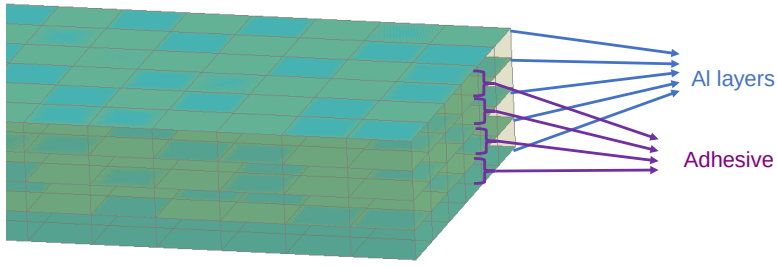

Fig. 9. FE model of laminated aluminum structure (for simplicity, only 5 aluminum layers are shown in the figure)

An automatic single surface contact was assigned to the fixture and aluminum layers to prevent any penetrations during loading. When modeling the axial drop test, a rigid hollow cube with the top surface removed was used as the axial fixture to secure the sample. The cube was 50 mm high to replicate the experimental setup.

In addition, a rigid flat plate was used as the impactor. To mimic the experimental setup for three-point bending, cylinders were modeled to represent the fixture and the impactor. These cylinders were all 45 mm in diameter and assigned a rigid material type to prevent deformation of the fixture. Single Point Constraints (SPC) were assigned to the fixtures to fix them in space. In addition, an SPC was used to fix the impactor in all 6 degrees of freedom, except the vertical drop direction [20]. This ensured the impact angle was perpendicular to the sample. The corresponding initial velocity was assigned to rigid impactors for each test condition. Fig. 10 displays the axial and three-point bending simulations.

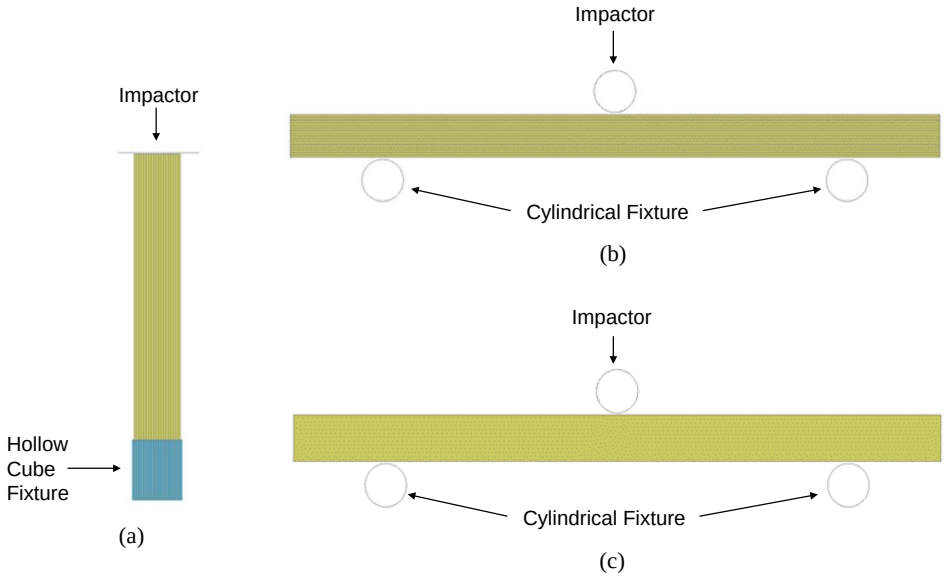

Fig. 10. (a) Axial drop model; (b) Normal drop model; (c) Transverse drop model

The force profiles were extracted and compared with the experimental results. By using the experimental force deflection results and high-speed videos of the events, the tiebreak contact parameters were calibrated and validated using a reverse engineering method to match the failure strengths, deformation, and delamination in the model for all three test conditions [18].

4. Results and discussion

4.1. Axial drop

Fig. 11a–c show photos of a LACS testing sample pre-post and during test. It is noted that buckling occurs during the test and the sample presents a large plastic deformation, which is considered as the dominate failure mode for laminated aluminum structures under axial loading. Fig. 11d and Fig. 11e present the

(a) (b) (c) (d) (e)

Fig. 11. (a) LACS sample pre-test; (b) LACS sample during axial drop test; (c) LACS sample post axial drop test; (d) simulated LACS before applied load; (e) simulated LACS after removed load

simulation results before and after the load is applied. A large plastic deformation with non-linear buckling is also observed.

Fig. 12a shows a top view of the post-test sample, where delamination is observed. Fig. 12b shows the simulation results in a top view, where small delam-

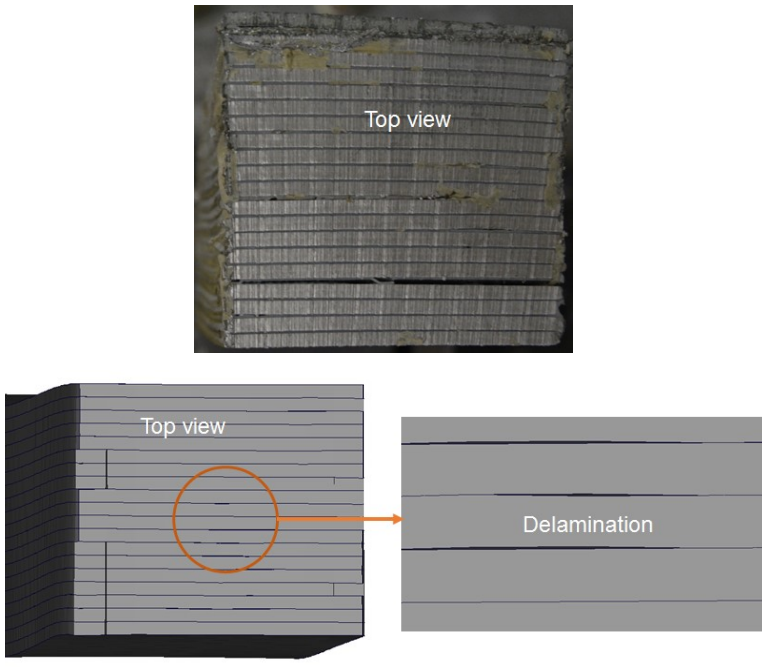

(a) (b)

Fig. 12. (a) Observed delamination in a post-test LACS; (b) predicted delamination in the simulation

ination is also predicted. The delamination can reduce the structure's integrity and stiffness and thus the critical buckling load.

For the experimental data discussed in this study, S# stands for the test sample number and -Axial, -Normal, or -Transverse indicates the type of loading the sample underwent. Fig. 13 compares the experimental (S1-Axial and S2-Axial) and simulated force-time curves. It is noted that before buckling occurs, the force in the elastic region is similar between the experimental and simulation results. The critical buckling load (peak load in the force-time curve) predicted by the simulation was slightly higher than the experiment. This can be due to the variation of material properties between the material model used in the simulation and the experimental samples. The second possible reason for the mismatch between the simulation and the experiments is the initial delamination existing in the experimental samples. This delamination can be caused by several factors. One of them is the joining techniques. During the preparation process, the adhesive may not be uniformly distributed between two aluminum layers. In addition, there can be voids and bubbles in the adhesive. Even though this initial delamination is local, it affects the structure's integrity and reduces its stiffness.

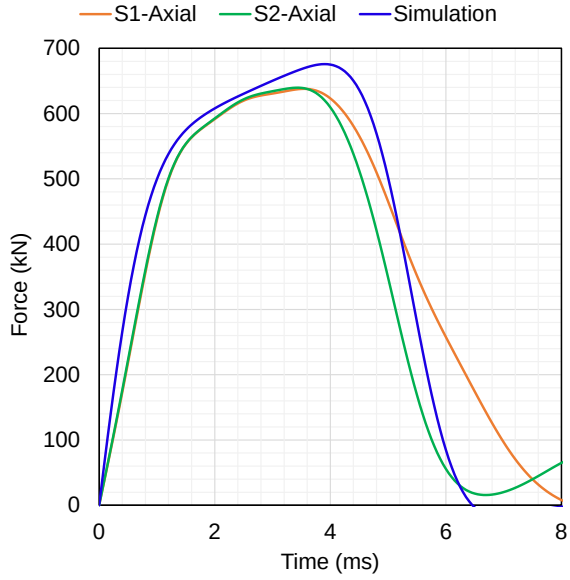

Fig. 13. Force-time curve comparison between experiments and the simulation

For a free-fixed column (free at one end, and fixed at the other end), buckling will occur around the axis with the lower moment of inertia. The axial samples possessed a rectangular column cross section, and they buckled around the y axis. This is because the moment of inertia around the y axis was smaller than the one around z axis, shown in Fig. 14a. To understand the buckling behavior of LACS with different rectangular cross sections, the structure's width (y direction)

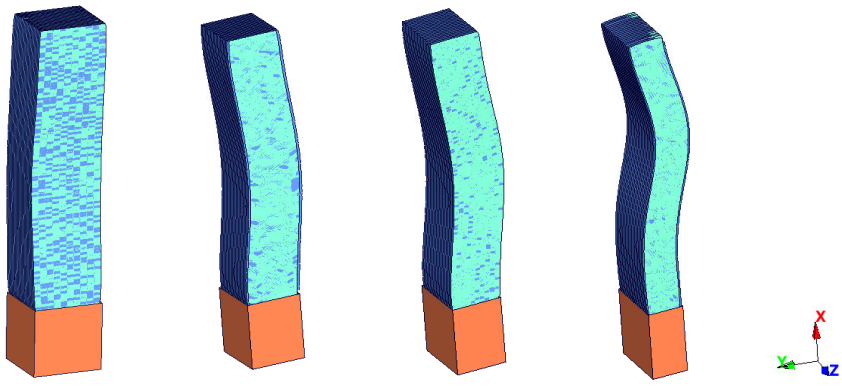

Fig. 14. (a) Axial compression buckling around Y-axis (SF of 1); (b)–(d) axial compression buckling around Z-axis having reduced structure's width with SFs of 0.8, 0.7, and 0.5, respectively

was varied using scale factors (SFs) of 0.5, 0.7 and 0.8. Due to the testing cost limitations, only simulations were performed in this study. Fig. 14b–d show the buckling mode with the SFs of 0.5, 0.7 and 0.8, respectively. It is noted that, when the SFs are applied, the structure buckles along the z axis, since the moment of inertia around it is smaller. Additionally, the structure with the smallest cross section (SF of 0.5) shows larger buckling deformation, which is expected as it had a lower critical buckling load. Fig. 15 compares the force-time curves. It is noted that structures with smaller cross sections yield lower peak loads but require more

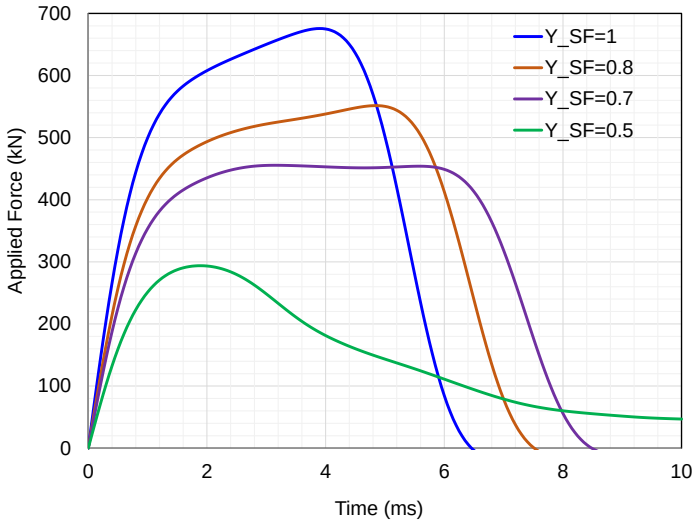

Fig. 15. Simulated force-time curves for structure's cross-section having varied structure's widths (SFs of 1, 0.8, 0.7 and 0.5)

time to absorb the impact energy and reduce the impactor's velocity to zero. This can also be seen from Fig. 16, which compares the impactor's kinetic energy-time curves.

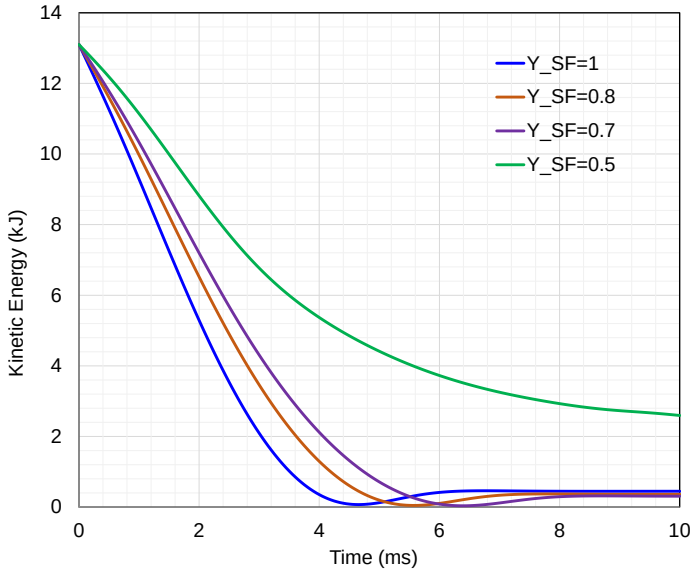

Fig. 16. Simulated impactor kinetic energy-time curves for structure's cross-section having varied structure's widths

4.2. Normal three-point bending drop tests and simulation

Fig. 17 compares the failure modes observed in the experiments and the simulation under normal three-point drop bending. It can be seen that the simulation successfully captures the failure modes: large plastic deformation; local buckling on top aluminum layers; delamination between bottom aluminum layers; and fracture on bottom aluminum layers.

Fig. 18 compares the simulated force-time curve to the experiments for the normal three-point drop bending tests. The simulation and experiments yielded slightly different peak force magnitudes, but at the same corresponding time. As discussed in the previous section, the material model used in the simulation does not consider the strain rate effect, which can cause lower peak force in the simulation. Additionally, the experimental samples do not have the exact geometrical dimensions and material properties used in the simulation, which can contribute to this difference. The load drop in each corrugation is associated with crack propagation through the adhesive towards the interfaces between aluminum and adhesive. The crack in adhesive can be initiated by the shear stress. After initial drop, the load did not decrease further as displacement increases. However, as the delamination (interfacial failure) reduces the structure's stiffness, the peak load in each corrugation

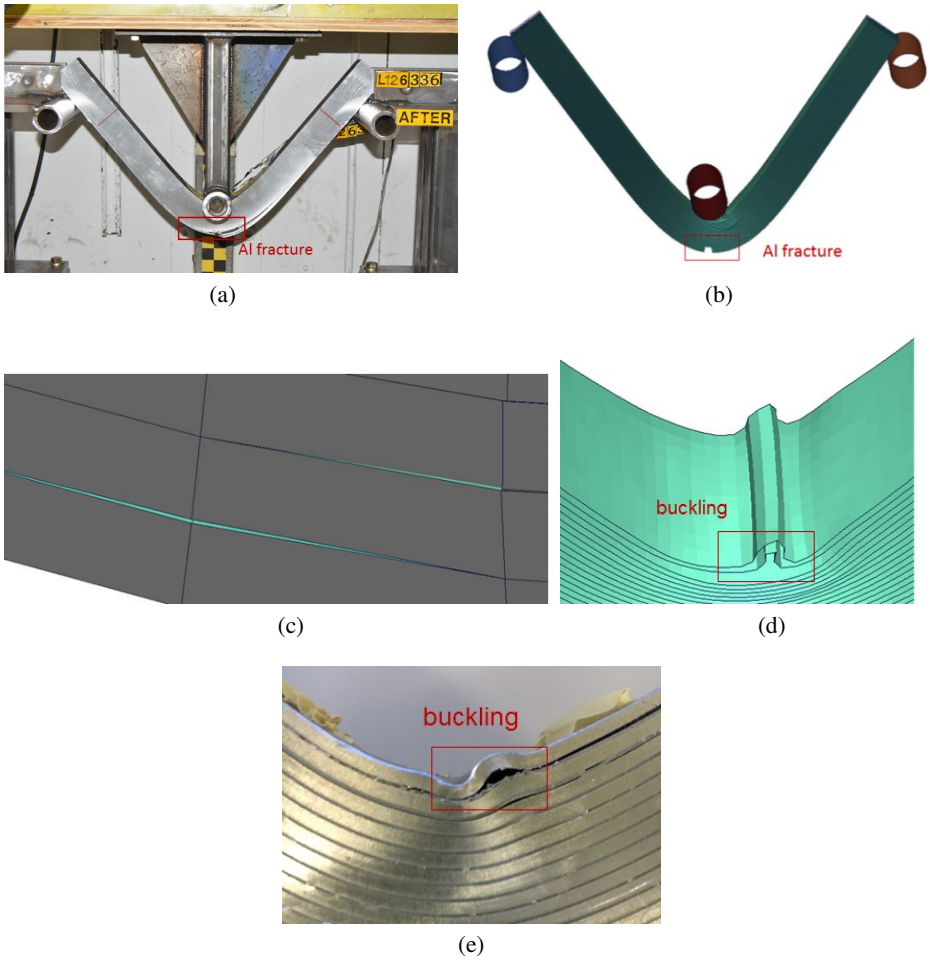

Fig. 17. (a) Observed large plastic deformation and fracture on bottom aluminum layers in experiments; (b) predicted large plastic deformation and aluminum fracture on bottom aluminum layers; (c) delamination between bottom aluminum layers in the simulation; (d) predicted local buckling on top aluminum layers in the simulation; (e) observed local buckling on top aluminum layers in experiments

decreases. This pattern of crack propagation, delamination and displacement increase creates the multiple corrugations in the experimental force-time curve. In the present study, the crack propagation process is not considered in the simulations, that makes the simulated force-time curve smoother. This can also be seen in the transverse three-point drop force-time curves in next section. The degradation of force over time was similar between the simulation and experiments. Overall, the simulation and experiments showed a good agreement.

Fig. 19 shows the plastic strain distribution in the aluminum and adhesive from the simulation. It is noted that the maximum plastic strain in the aluminum

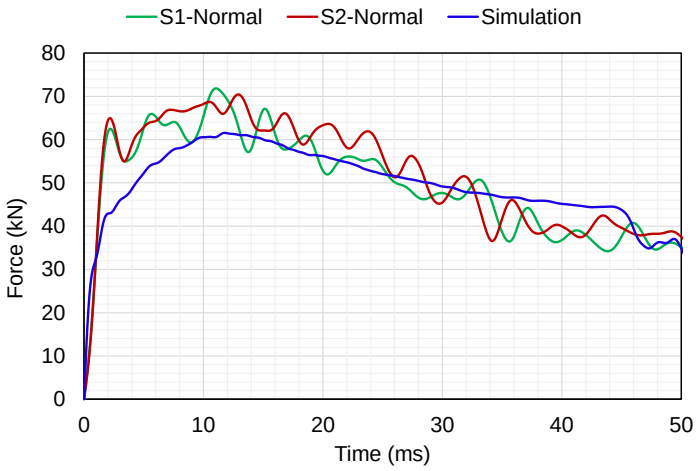

Fig. 18. Force-time curve comparison between experiments and the simulation in normal three-point drop bending

occurred at the top and bottom layers near the center of the span. This strain is induced by compressive stresses at the top aluminum layers and tensile stresses at the bottom aluminum layers. These stresses were created from the applied bending moment and have a maximum magnitude at the center of the span, where the bending moment is the maximum. Contrastingly, the maximum plastic strain for the adhesive occurs at the center of the span, but in the middle layers. This strain is produced by the shear stress, which is the maximum at the neutral axial and decreases towards the top and bottom layers.

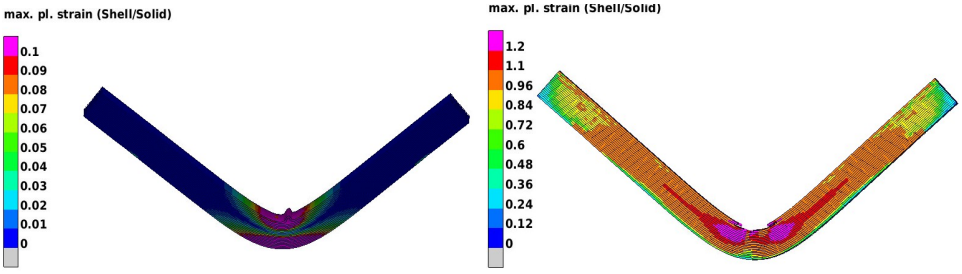

(a) (b)

Fig. 19. Simulation results of structure subjected to normal three-point drop bending: (a) equivalent plastic strain in aluminum; (b) equivalent plastic strain in adhesive

4.3. Transverse three-point bending drop tests and simulation

Fig. 20a and Fig. 20b present the large plastic deformation observed in the simulation and experiments for LACS during transverse three-point bending. There was no fracture of the aluminum, but there was delamination between multiple

(a)

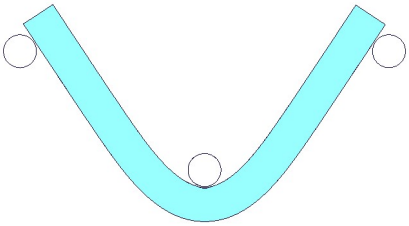

(b)

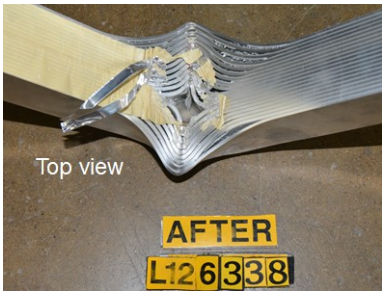

(c)

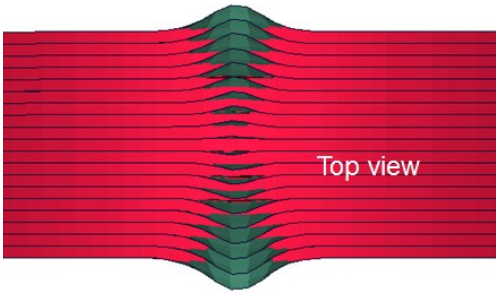

(d)

Fig. 20. (a) Observed large plastic deformation in the experiment; (b) predicted large plastic deformation in the simulation; (c) observed delamination and local buckling at the center of span in the experiment; (d) predicted delamination and local buckling at the center of span in the simulation

aluminum layers in the impact region, shown in Fig. 20c. Fig. 20d shows the predicted delamination in the impact region.

Fig. 21 compares the simulated force-time curve to the experimental curves for transverse three-point drop bending. Similar to the normal three-point drop bending results, the peak force in the simulation is a little smaller than the ones in the experiments. The plateau in the experimental force-time curves between 2–15 ms indicates the delamination process between the aluminum layers in the impact region [24]. The simulation shows a slower force reduction compared to the experiments. A possible reason for this difference is the delamination area, which is larger in the experiments when compared to the simulation. As discussed in the axial drop section, initial delamination can be created in the testing samples during the sample preparation process. The compressive stress at the center of the span can cause local buckling, which results in a more progressive delamination [25]. Delamination will reduce the structure's bending stiffness, so the load force decreases quicker in the experiments than the simulation.

Fig. 22 shows the plastic strain distribution in the aluminum and adhesive from the simulation during transverse three-point bending. Similar to Fig. 19a, aluminum undergoes maximum plastic strain in the top and bottom regions at the center of the span, which is induced by the compressive stress at the top and tensile stress at the

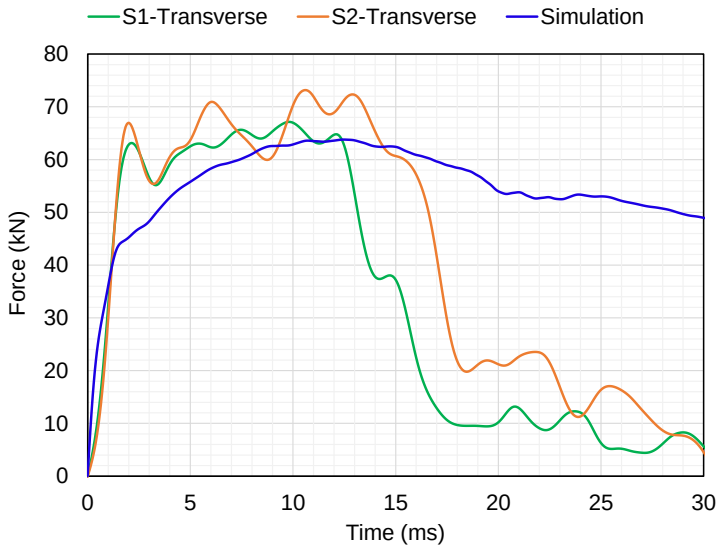

Fig. 21. Force-time curve comparison between the experiments and the simulation for transverse three- point drop bending

bottom. Unlike the normal three-point bending results shown in Fig. 19b, where the maximum plastic strain in the adhesive occurred at the center of span in the middle layers, the maximum plastic strain in the adhesive for transverse three-point bending occurred at the center of span and in the top region. It is noted that the large compressive stress in this region caused cohesive failure and suppressed the shear dominant failure [1].

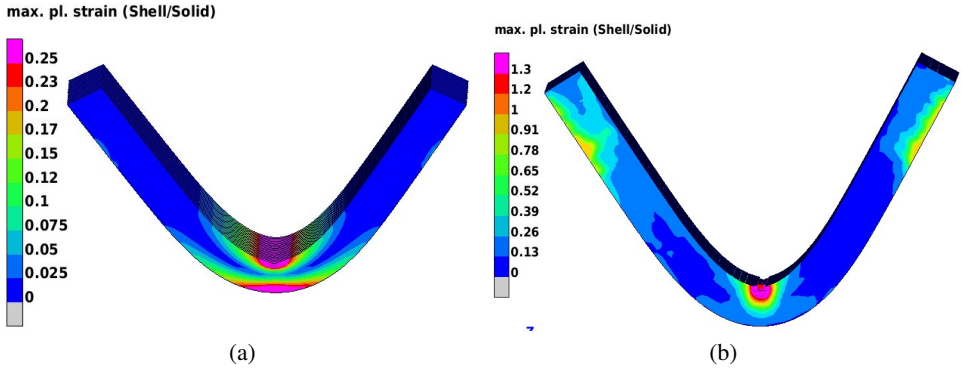

(a) (b)

Fig. 22. Simulation results of structure subjected to transverse three-point drop bending: (a) equivalent plastic strain in aluminum; (b) equivalent plastic strain in adhesive

5. Conclusions

The impact response of LACS consisting of 20 aluminum layers joined by the selected tape adhesive was investigated numerically and experimentally. Three impact tests (axial drop, normal and transverse three-point bending drop tests) were conducted in order to understand the LACS performance and failure modes. The peak load and various LACS failure modes were successfully predicted in the simulations. The main impact responses of Laminated Aluminum Composite Structure are as follows:

- For the axial drop impact, a large plastic deformation with non-linear buckling was observed, which is considered as the dominate failure mode for LACS under axial loading. Delamination was also present in the post-test LACS, which affected the sample's integrity and reduced its stiffness. Buckling direction in LACS was dependent on the moment of inertia along different axes.
- For the normal three-point drop bending tests, the failure modes of large plastic deformation, wrinkling on the top aluminum layers, delamination, and fracture on the bottom aluminum layers were observed. The wrinkling and fracture on aluminum layers were due to the compressive and tensile stresses from the bending moments. These stresses caused the maximum plastic strain to occur at the top and bottom layers in the aluminum. For adhesive, the maximum plastic strain occurred in the middle layers, which was caused by the shear stress.
- For the transverse three-point bending tests, the failure modes of large plastic deformation, delamination, and local buckling on the top aluminum layers were observed. The local buckling was induced by the compressive stress from the bending moments, and the maximum plastic strain occurred on the top and bottom aluminum layers. However, unlike the normal three-point bending, the maximum plastic strain in the adhesive for transverse three-point bending occurred in the top region. The large compressive stress in this region caused cohesive failure and suppressed the shear dominant failure.

Manuscript received by Editorial Board, February 07, 2020;
final version, April 22, 2020.

References

[1] D. Zangani, M. Robinson, and A.G. Gibson. Evaluation of stiffness terms for z-cored sandwich panels. *Applied Composite Materials*, 14:159–175, 2007. doi: 10.1007/s10443-007-9038-y.

[2] J. Yu, E. Wang, J. Li, and Z. Zheng. Static and low-velocity impact behavior of sandwich beams with closed-cell aluminum-foam core in three-point bending. *International Journal of Impact Engineering*, 35(8):885–894, 2008. doi: 10.1016/j.ijimpeng.2008.01.006.

[3] Q. Sun, Z. Meng, G. Zhou, S.-P. Lin, H. Kang, S. Keten, H. Guo, and X. Su. Multi-scale computational analysis of unidirectional carbon fiber reinforced polymer composites under various loading conditions. *Composite Structures*, 196:30–43, 2018. doi: 10.1016/j.compstruct.2018.05.025.

[4] G.S. Dhaliwal and G.M. Newaz. Modeling low velocity impact response of carbon fiber reinforced aluminum laminates (CARALL). *Journal of Dynamic Behavior of Materials*, 2:181–193, 2016. doi: 10.1007/s40870-016-0057-3.

[5] G.-C. Yu, L.-Z. Wu, L. Ma, and J. Xiong. Low velocity impact of carbon fiber aluminum laminates. *Composite Structures*, 119:757–766, 2014. doi: 10.1016/j.compstruct.2014.09.054.

[6] M. Koc, F.O. Sonmez, N. Ersoy, and K. Cinar. Failure behavior of composite laminates under four-point bending. *Journal of Composite Materials*, 50(26): 3679–3697, 2016. doi: 10.1177/0021998315624251.

[7] A. Shojaei, G. Li, P.J. Tan, and J. Fish. Dynamic delamination in laminated fiber reinforced composites: A continuum damage mechanics approach. *International Journal of Solid and Structures*, 71:262–276, 2015. doi: 10.1016/j.ijsolstr.2015.06.029.

[8] J. Wang, R. Bihamta, T.P. Morris, and Y.-C. Pan. Numerical and experimental investigation of a laminated aluminum composite structure. *Applied Composite Materials*, 26:1177–1188, 2019. doi: 10.1007/s10443-019-09773-7.

[9] D. Zangani, M. Robinson, and A.G. Gibson. Energy absorption characteristics of web-core sandwich composite panels subjected to drop-weight impact. *Applied Composite Materials*, 15:139–156, 2008. doi: 10.1007/s10443-008-9063-5.

[10] Q.-R. Yang, J.-X. Liu, S.-K. Li, and T.-T. Wu. Bending mechanical property and failure mechanisms of woven carbon fiber-reinforced aluminum alloy composite. *Rare Metals*, 35(12): 915–919, 2016. doi: 10.1007/s12598-014-0271-x.

[11] M. Kinawy, R. Butler, and G.W. Hunt. Bending strength of delaminated aerospace composites. *Philosophical Transactions of The Royal Society*, 370:1780–1797, 2012. doi: 10.1098/rsta.2011.0337.

[12] C. Kabogu, I. Mohagheghian, J. Zhou, Z. Guan, W. Cantwell, S. John, B.R.K. Blackman, A.J. Kinloch, and J.P. Dear. High-velocity impact deformation and perforation of fibre metal laminates. *Journal of Materials Science*, 53:4209–4228, 2018. doi: 10.1007/s10853-017-1871-2.

[13] X. Wang, X. Zhao, Z. Wu, Z. Zhu, and Z. Wang. Interlaminar shear behavior of basalt FRP and hybrid FRP laminates. *Journal of Composite Materials*, 50(8):1073–1084, 2016. doi: 10.1177/0021998315587132.

[14] C. Liu, D. Du, H. Li, Y. Hu, Y. Xu, J. Tian, G. Tao, and J. Tao. Interlaminar failure behavior of GLARE laminates under short-beam three-point-bending load. *Composites Part B: Engineering*, 97:361–367, 2016. doi: 10.1016/j.compositesb.2016.05.003.

[15] A. Yapici and M. Metin. Effect of low velocity impact damage on buckling properties. *Engineering*, 1:161–166, 2009. doi: 10.4236/eng.2009.13019.

[16] J. Sarkar, T.R.G. Kutty, D.S. Wilkinson, J.D. Embury, and D.J. Lloyd. Tensile properties and bendability of T4 treated AA6111 aluminum alloys. *Materials Science and Engineering: A*, 369(1-2):258–266, 2004. doi: 10.1016/j.msea.2003.11.022

[17] 3M Automotive Division, 3M TM Structureal Adhesive Tape SAT1010M Technical Data Sheet, 3M, St. Paul, 2019.

[18] C.J. Corbett, L. Laszczyk, and O. Rebuffet. Assessing and validating the crash behavior of Securalex HS, a high-strength crashworthy aluminum alloy, using the GISSMO model. In 14th International LS-Dyna Users Conference, Detroit, 2016.

[19] G. Falkinger, N. Sotirov, and P. Simon. An investigation of modeling approaches for material instability of aluminum sheet metal using the GISSMO-model. In 10th European LS-DYNA Conference, Wurzburg, 2015.

[20] Livermore Softwar Technology Corporation (LSTC), LS-DYNA ® KEYWORD USER'S MANUAL VOLUME II Material Models, 2012.

[21] A. Mostafa, K. Shankar, and E.V. Morozov. Experimental, theoretical and numerical investigation of the flexural behaviour of the composite sandwich panels with PVC foam core. *Applied Composite Materials*, 21:661–675, 2014. doi: 10.1007/s10443-013-9361-4.

[22] G.A.O. Davies and I. Guiamatsia. The problem of the cohesive zone in numerically simulating delamination/debonding failure modes. *Applied Composite Materials*, 19:831–838, 2012. doi: 10.1007/s10443-012-9257-8.

[23] F. Dogan, H. Hadavinia, T. Donchev, and P.S. Bhonge. Delamination of impacted composite structures by cohesive zone interface elements and tiebreak contact. *Central European Journal of Engineering*, 2(4):612–626, 2012. doi: 10.2478/s13531-012-0018-0.

[24] C. Hesch and P. Betsch. Continuum mechanical considerations for rigid bodies and fluid-structure interaction problems. *Archive of Mechanical Engineering*, 60(1):95–108, 2013. doi: 10.2478/meceng-2013-0006.

[25] J.J.C. Remmers and R. de Borst. Delamination buckling of fibre-metal laminates. *Composites Science and Technology*, 61(15):2207–2213, 2001. doi: 10.1016/S0266-3538(01)00114-2.